Palaeogeography, Palaeoclimatology, Palaeoecology 514 (2019) 156–167

Contents lists available at ScienceDirect

Palaeogeography, Palaeoclimatology, Palaeoecology

journal homepage: www.elsevier.com/locate/palaeo

Geochemistry and isotopic study of southern Bay of Bengal sediments: Implications for provenance and paleoenvironment during the middle Miocene

Barnita Banerjee[a], S. Masood Ahmad[a,c,*], E.V.S.S.K. Babu[a], V.M. Padmakumari[b], S. Kumar Beja[a], M. Satyanarayanan[a], A. Keshav Krishna[b]

[a] Academy of Scientific and Innovative Research (AcSIR), CSIR-National Geophysical Research Institute, Hyderabad 500 007, India
[b] CSIR-National Geophysical Research Institute, Hyderabad 500 007, India
[c] Department of Geography, Faculty of Natural Sciences, Jamia Millia Islamia, New Delhi 110025, India

ARTICLE INFO

Keywords:
Marine sediments
Terrigenous fluxes
Trace elements
Indian summer monsoon
Redox conditions
Productivity

ABSTRACT

The Bay of Bengal (BoB), the largest bay in the world, is known to receive large amounts of fresh water and suspended particulate matter from different sources. The sediments deposited in the bay serve as a repository for paleoenviromental reconstruction studies. The Miocene Epoch is an important interval in geologic time as it is marked by major climatic events that controlled ocean productivity, redox conditions and provenance of sediments. However, limited work has been carried out to establish paleoenviromental changes and provenance of sediments during the Miocene. Here we present detailed geochemical and radiogenic (Sr, Nd) isotopic results from predominantly middle Miocene sediments of Ocean Drilling Program (ODP) Site 758A, located in the southern BoB (Lat. 5 °23′N, Long. 90°21′E; water depth 2925 m), to understand paleoredox conditions, paleoproductivity and provenance. The results suggest that these sediments are strongly linked to climatically modulated surface processes that affected the region.

The distribution of redox-sensitive element proxies (U, V, Cr) at interval ~17–8 Ma points to an oxic depositional environment. The major, trace and rare earth elements distribution supports prevalence of the Indian summer monsoon (ISM) at ~12–10 Ma. Productivity proxies (Ba_{bio}, P_{org}) show a decreasing trend during colder events (East Antarctic Ice Sheet expansion – EAIS and advent of late Miocene cooling – LMC events). The trace and rare earth element concentrations are generally low, except at intervals where glass shards were found. The $^{87}Sr/^{86}Sr$ and $\varepsilon_{Nd}(0)$ values indicate that the sediments belong to the High Himalayan sedimentary series (HHSS) throughout the middle Miocene. However, prior to initiation of the ISM, these sediments underwent meteoric alteration in the lowlands before deposition in the BoB. Our records suggest that sediments at ODP Site 758A may have been introduced into the BoB through the Irrawaddy-Yarlung-Tsangpo drainage system during the entire period of this study. The Irrawaddy-Yarlung-Tsangpo system drained the Indus-Tsangpo Suture zone, southern Tibet, the eastern Himalayas and the Arakan coast before debouching in the BoB.

1. Introduction

The Bay of Bengal (BoB) receives abundant fresh water and suspended particulate matter, from the Himalayan (Ganges – Brahmaputra), Tibetan (Irrawaddy and Salween) and peninsular (Mahanadi, Krishna-Godavari, Cauvery) rivers (Bird et al., 2008). These rivers are the primary transporters of physically and chemically weathered continental materials to the ocean. Intense Indian Summer Monsoon (ISM) causes high runoff in the river basins, which in turn enhances erosion in the catchment area resulting in accumulation of sediments and metasediments (2.88×10^{16} tonnes) in Bengal Fan (Curray, 1994). On the basis of chemical and isotopic properties of sediments, several investigators argued that physical erosion in these river are regulated by climate (Singh and France-Lanord, 2002; Singh et al., 2008; Chakrapani and Saini, 2009). Further, the erosion and weathering patterns of these river basins and their spatio-temporal variations have been extensively studied due to their key role in the global carbon budget which in turn regulates the climate (Dalai et al., 2002; Das et al., 2005; Singh et al., 2005; Rahaman et al., 2009; Huh, 2010).

* Corresponding author at: Academy of Scientific and Innovative Research (AcSIR), CSIR-National Geophysical Research Institute, Hyderabad 500 007, India.
E-mail address: smasoodahmad@rediffmail.com (S. Masood Ahmad).

https://doi.org/10.1016/j.palaeo.2018.10.022
Received 27 February 2018; Received in revised form 22 October 2018; Accepted 22 October 2018
Available online 24 October 2018
0031-0182/ © 2018 Elsevier B.V. All rights reserved.

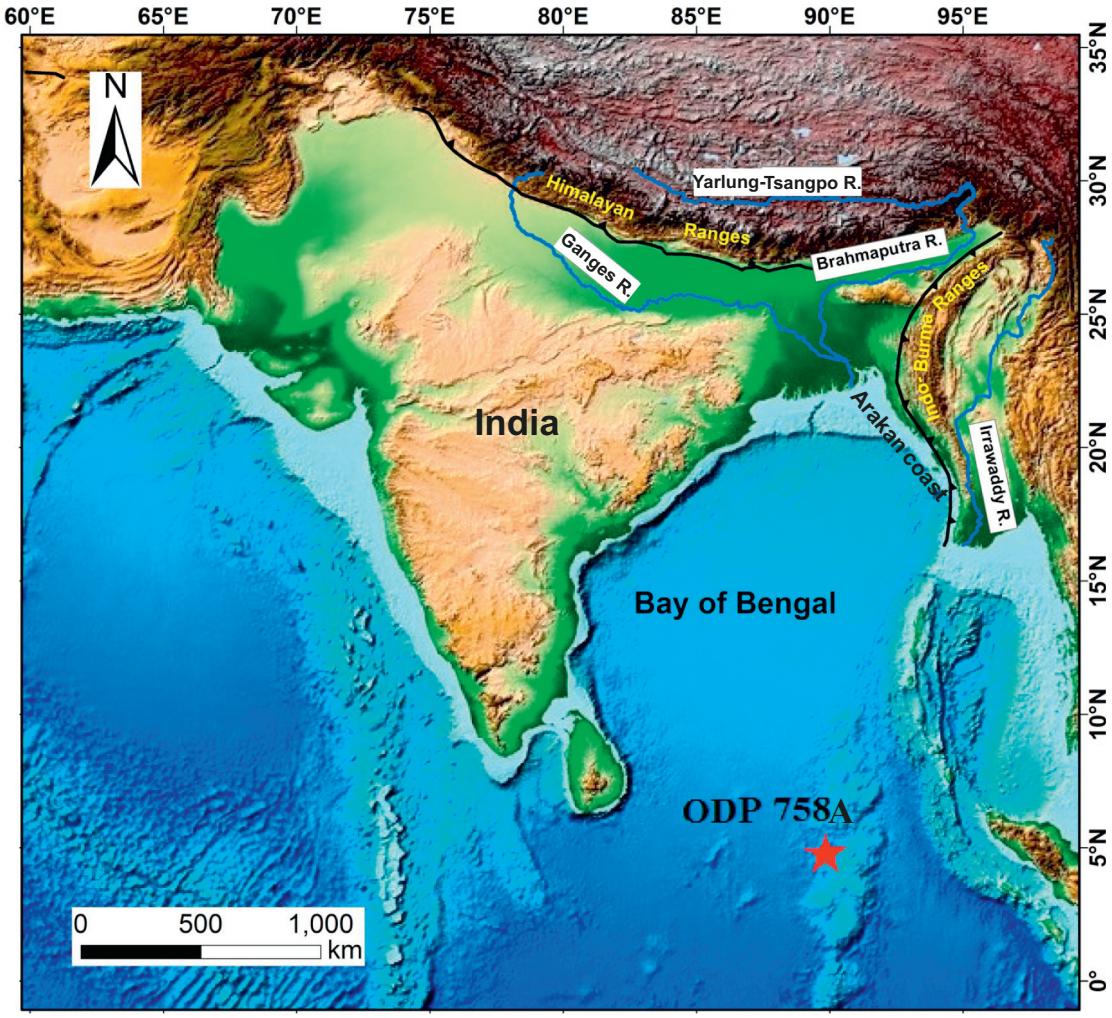

Fig. 1. Location map of ODP Site 758A. The main river systems and potential source areas are marked. (Source: http://www.ngdc.noaa.gov/mgg/image/color_etopo1_ice_low.jpg).

The Miocene Epoch is an important interval in geologic time as it is marked by major climatic events like Miocene Climatic Optimum (17–15 Ma), East Antarctic ice sheet (EAIS) expansion and global cooling event at 13.9 Ma (Flower and Kennett, 1993, 1995; Holbourn et al., 2005, 2007, 2014, 2015) and initiation of the ISM. The Miocene Epoch is also marked by major tectonic events in the Himalayas which might have enhanced the erosion and weathering processes over the Himalayan river basins which in turns regulates the global carbon budget and monsoonal downpour (Crowley et al., 1998; Dettman et al., 2003; Anderson and Wellner, 2013; Tremblay et al., 2015). Sediment archived in the BoB can provide useful information on tectonic-erosion-climate link, paleoproductivity and paleoredox conditions. We focused on the southern BoB because limited work has been attempted in this region to understand the biological and physical processes that occurred during the middle Miocene.

The responses of the Quaternary sediments in the BoB to fluctuations in riverine inputs have been investigated to reconstruct the erosional pattern of river basins from the Himalaya and peninsular India. Radiogenic isotopes on Quaternary sediments suggest that they were derived from different sources, which in turn have been attributed to variability in wind direction and intensity of summer and winter monsoon systems (Ahmad et al., 2005a; Kessarkar et al., 2005). The clay mineralogy of the BoB sediments indicated that the ISM was stronger in warmer periods and weaker in colder periods during the Holocene (Subramanian, 1987; Kolla and Rao, 1990). The ISM, however, was initiated in the Miocene Epoch and no records of paleoenviromental changes and provenance of sediments were available in Miocene. In this study we have attempted a similar approach used in Quaternary sediments to determine the timing of development of modern like conditions in the past. Several researchers proposed that the Asian monsoon system was intensified at around 8 Ma (Prell and Kutzbach, 1992; Chen et al., 2003; Wan et al., 2007). However, this view has been challenged by others and suggested that the intensification of monsoon occurred in early Miocene (Jia et al., 2003) or late Eocene (Licht et al., 2014). The freshwater discharge in the BoB and wind induced upwelling associated with the ISM is responsible for nutrient supply resulting in increase in primary productivity (Ramaswamy and Nair, 1994; Gupta et al., 2004), decrease in salinity and strong stratification (Östlund et al., 1980). Therefore, it is necessary to understand the implications of these parameters on behaviour and distribution of redox-sensitive elements, to establish the terrigenous input, productivity changes and provenance in middle Miocene.

In this study we present major and trace element geochemistry along with strontium (Sr) and neodymium (Nd) isotope data of Miocene sediments from Ocean Drilling Program (ODP) Site 758A. We have used K/Al, $^{87}Sr/^{86}Sr$ and $\varepsilon_{Nd}(0)$ to provide information on the relative contribution of terrigenous detrital matter derived from different provenances (Wehausen and Brumsack, 1999) and weathering intensity (Schneider et al., 1997). Furthermore, variation in biological productivity in the BoB was reconstructed using biogenic barium (Ba_{bio})

(Dehairs et al., 1980; Dymond et al., 1992; Schoepfer et al., 2015) and organic phosphorus (P_{org}) (Delaney, 1998; Schoepfer et al., 2015). Abundance of redox-sensitive element uranium (U), vanadium (V) and chromium (Cr) (Calvert and Pedersen, 1993) has been used to decipher depositional conditions. The chemostratigraphy and biostratigraphy provide a chronological framework to interpret changes in sediment geochemistry at ODP Site 758A (Ahmad et al., 2005a; Banerjee et al., 2017). A comparison of geochemical elemental data together with foraminiferal oxygen isotope curve may provide information about the relationship between terrigenous input, monsoons, sea-level changes and climate. Although the present work represents a coarser resolution, yet this is a first attempt to reconstruct past depositional environment and paleoproductivity in the southern BoB, based on geochemical and isotopic tracers.

2. Material and methods

The ODP Site 758A is located on the Ninetyeast Ridge in the southern BoB (Lat. 5°23′N, Long. 90°21′E; water depth 2925 m) (Fig. 1). The major constituents of sediments at this site are calcium carbonate ($CaCO_3$), which increases downcore to > 80% at 121–296 mbsf with minor amounts of terrigenous silt, clay and volcanic tephra (Farrell and Janecek, 1991). The sampling resolution is ~0.1 Myr in the study interval, but is low at ~14 Ma, due to unavailability of enough sediment samples for major element analysis. A total of 46 samples were selected for analysis of major oxides and trace elements including rare earth elements (REEs). Isotopic ratios ($^{87}Sr/^{86}Sr$ and $\varepsilon_{Nd}(0)$) were carried out in 19 samples only.

Sediment samples were powdered in an agate mortar followed by intermittent cleaning and drying of agate mortar with acetone to avoid sample cross contamination. Major element concentrations were determined by X-ray fluorescence spectrophotometer (XRF; Philips MAGIX PRO® Model 2440) with precision obtained for most of the major oxides were < 3% (details provided in Table S3) (Krishna and Govil, 2007). Trace elements and REEs were determined by High Resolution Inductively Coupled Plasma Mass Spectrometer (HR-ICP-MS) (Nu Instruments Attom®, UK) at CSIR-National Geophysical Research Institute (NGRI), Hyderabad. The samples were dissolved through acid refluxing. A mixture of 7:3 HF-HNO_3 was added to 0.05 g of sediment powder and kept on a hot plate at 150 °C for 48 h. The entire mixture was dried on hot plate. When the sample was almost dry, it was dissolved by adding 10 ml of 1:1 HNO_3 and the solution was kept on hot plate for 10–15 min. Then 5 ml Rh solution (1 ppm) was added to it as an internal standard. After cooling, the volume of the solution was made up to 250 ml. Geochemical reference standards MAG I, MESS 3 and HISS I were used for ICP-MS analysis of samples (Satyanarayanan et al., 2014). The Ce/Ce* ratio was calculated following the equation of Bau and Dulski (1996). In this study we have normalised trace and REEs with upper continental crust because the degree of enrichment or depletion of a trace element in a sample is evaluated relative to its concentration in a reference (McLennan, 2001).

The equation for elemental excess was determined by calculating:

$$E_{excess} = E_{total} - E_{terrigenous} \quad (1)$$

$$E_{terrigenous} = Al_{total} \times (E/Al)_{detrital} \quad (2)$$

The $(E/Al)_{detrital}$ is considered that of the average upper continental crust, where Al denotes aluminium content (McLennan, 2001). The average $(Ba/Al)_{detrital}$ value of the upper continental crust is considered as 0.0065 (McLennan, 2001). However, due to potential influence of riverine inputs at our study site (Reitz et al., 2004) we have used average Ba/Al ratios from surface sediments (< 10 cm) of a core from the BoB (Babu et al., 2010). A $(Ba/Al)_{detrital}$ value of 0.01 is used for this study to calculate the Ba_{bio} content. The P/Al ratio of the upper continental crust (0.0087) has been used to infer P_{org} content (McLennan, 2001). Mass accumulation rate (MAR) of the element or elemental flux (E_{excess} flux) were estimated by,

$$E_{excess}\ flux = (E_{excess}/100) \times \rho_{dry} \times LSR \quad (3)$$

E_{excess} flux is expressed in $g\,cm^{-2}\,kyr^{-1}$, dry bulk density ρ_{dry} in mg/cm^3 and linear sedimentation rate (LSR) in cm/kyr. The dry bulk density was obtained by interpolating the dry bulk density reported earlier in the Initial Report of Leg 121, ODP Site 758A (Peirce et al., 1989). LSR was calculated by age-depth model of ODP Site 758A (Ahmad et al., 2005b; Banerjee et al., 2017).

Elemental enrichment factors (E_{EF}) were calculated by (Tribovillard et al., 2006):

$$E_{EF} = E/Al_{sample}/E/Al_{crust} \quad (4)$$

The Sr and Nd isotopic ratios were determined from the carbonate free fraction to analyse the provenance of sediments at ODP Site 758A. The samples were treated with a solution of 3% hydrogen peroxide to remove organic carbon, decarbonated with 1 M HCl and washed thoroughly with milli-Q water (Ahmad et al., 2005a). Isotopic measurements were carried out on VG-354E Thermal Ionization Mass Spectrometer (TIMS) in the dynamic triple collector mode at CSIR-NGRI, Hyderabad. The $^{87}Sr/^{86}Sr$ values were corrected for fractionation with $^{86}Sr/^{88}Sr = 0.1194$; SRM-987 = 0.710210 ± 24 (2σ, $n = 15$). The $^{143}Nd/^{144}Nd$ ratios were corrected for fractionation with $^{146}Nd/^{144}Nd = 0.7219$ and normalised to La Jolla Nd = 0.511850 ± 10 (2σ, $n = 12$). Blank contribution in the Sr (< 250 pg) and Nd (< 25 pg) isotope measurement was negligible. The age model presented here is based on nannofossil events and interpolated numerical ages (Klootwijk et al., 1992). The biostratigraphic age model of ODP Site 758A shows a reasonably good agreement with Sr isotope derived chemostratigraphy (< ± 1.48 Ma), based on best fit trend of $^{87}Sr/^{86}Sr$ with time (Ahmad et al., 2005b; Banerjee et al., 2017) using polynomial regression of Hodell et al. (1991) and Miller et al. (1991) (Fig. S1).

3. Results

The Ba_{bio} concentrations were converted to their respective fluxes (using Eq. (3)) that ranged between 5.6 $g\,cm^{-2}\,kyr^{-1}$ to 0.07 $g\,cm^{-2}\,kyr^{-1}$ (Fig. 2D) (Table S1). The P_{org} flux showed high variability ranging between 67.1 $g\,cm^{-2}\,kyr^{-1}$ to 0.65 $g\,cm^{-2}\,kyr^{-1}$ (Fig. 2F) (Table S1). The highest Ba_{bio} flux was observed at 10.4 Ma, whereas highest P_{org} flux was observed at 10 Ma. Both the proxies exhibit an increasing trend from ~12–10 Ma followed by a decreasing trend until 8 Ma. The total barium (Ba) content varies between 1446 and 216 μg/g and Ba_{bio} varies from 1112 to 13 μg/g suggesting an average of 57% of total Ba is of biogenic origin. In this study, U, V and Cr concentrations are used as redox-sensitive trace elements proxies. The U concentrations in sediments were low throughout the study interval (1.9–0.2 μg/g) (Fig. 4A). The U enrichment factor varied from 2.1 to 0.24 (Fig. 4B) with highest ratio of 2.1 at 15.5 Ma. The V enrichment factor showed less variation ranging between 0.8 and 0.2 (Fig. 4C), whereas Cr enrichment factor varied from 2 to 0.4 (Fig. 4D) (Table S1). All sediment samples exhibited negative Ce-anomaly relative to Post Archean Australian Shale (PAAS) with values ranging from 0.9 to 0.5 (Fig. 4E). K/Al ratio showed a shift from 0.09 to 0.14 at 12.3 Ma (Fig. 5C) (Table S1) and the average Al (%) also increased from 1.8% to 3.2% at 12.3 Ma (Fig. 5D). The $^{87}Sr/^{86}Sr$ ratios varied significantly between 0.716 and 0.709, whereas $\varepsilon_{Nd}(0)$ values varied between −5.46 and −15.45 (Fig. 6) (Table S2).

The PAAS normalised REEs pattern (after Taylor and McLennan, 1985) in three sediment samples (age ~ 10.6 Ma, 10.9 Ma and 11.2 Ma) showed high concentrations than rest of the samples (Fig. 8). The PAAS normalised pattern of these samples also exhibit anomalously high concentration for some trace metals like Sc, V, Cr, Co, Ni, Ga, Rb, Nb, Cs, Hf (Fig. 9).

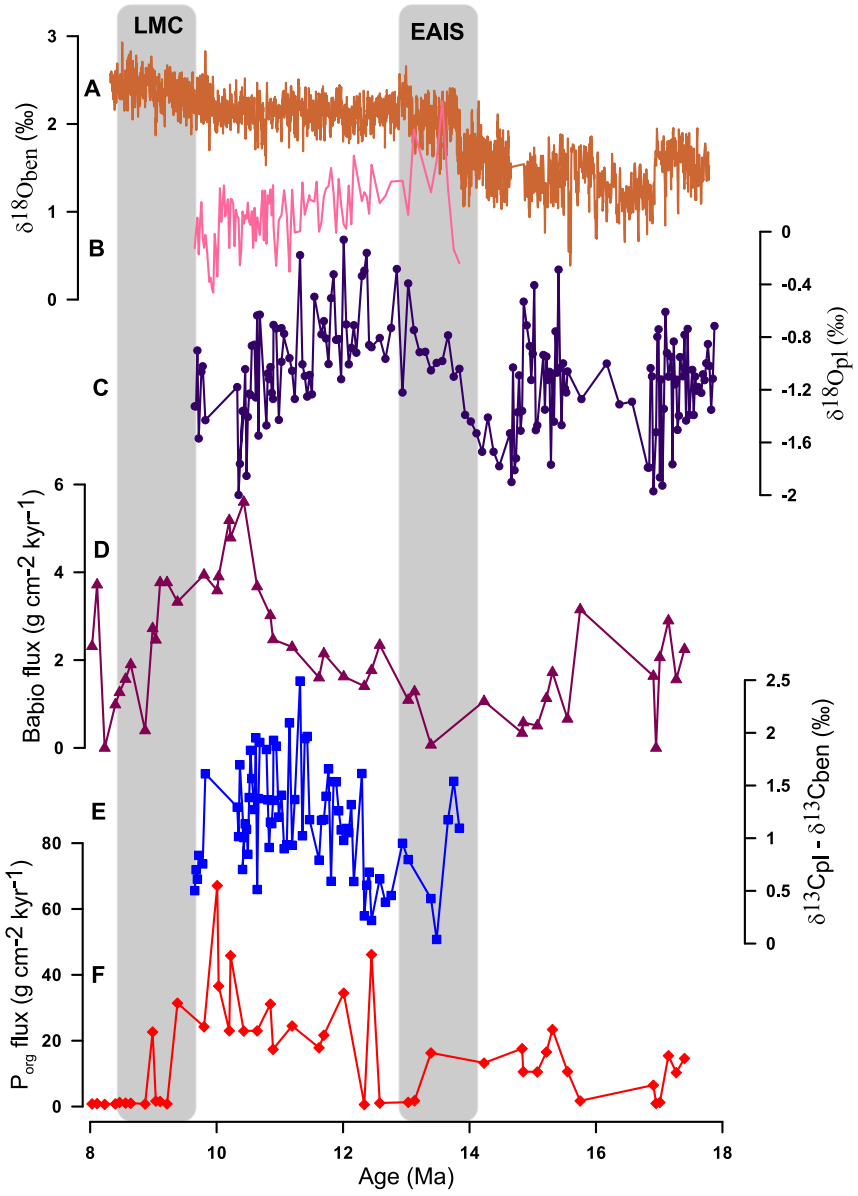

Fig. 2. (A) $\delta^{18}O_{ben}$ (‰) of Site 1146 (Holbourn et al., 2013), Site 1338 (Holbourn et al., 2014), Site 1337 (Holbourn et al., 2015), (B) $\delta^{18}O_{ben}$ (‰) value of ODP Site 758A (Banerjee et al., 2017), (C) $\delta^{18}O_{pl}$ (‰) value of ODP Site 758A, (D) Biogenic Barium (Ba_{bio}) flux (g cm^{-2} kyr^{-1}) (E) $\delta^{13}C_{pl}$-$\delta^{13}C_{ben}$ (‰) (Banerjee et al., 2017) of ODP Site 758A (F) Organic Phosphorus (P_{org}) flux (g cm^{-2} kyr^{-1}). The grey shaded area represents colder events (East Antarctic Ice Sheet – EAIS expansion and advent of Late Miocene cooling – LMC event).

4. Discussion

The sediments at ODP Site 758A contain low concentrations of trace elements and REEs due to carbonate dilution. A detailed microscopic study indicates presence of glass shards at ~11 Ma age suggesting a volcanic event at the proximity of the core site, may be at the Indonesian region during this period (Fig. S2). Volcanic glass shards may leach substantial amounts of alkali and alkaline earth elements, possibly from the entire volume of the tephra shards (Jones and Gislason, 2008; Tamburrino et al., 2012; Ponomareva et al., 2015; Rawson et al., 2015) leading to enrichment of trace and REEs in sediment samples. The trace elements, REEs and isotopic compositions of marine sediments at ODP Site 758A showed prominent shifts during the period of study. We have compared our geochemical record with the previously published stable isotope ($\delta^{13}C$ and $\delta^{18}O$) records from the same site (Banerjee et al., 2017) and also from global ocean cores (Holbourn et al., 2013, 2014, 2015). Our results indicate climatic events along with tectonics played a major role for significant changes in weathering pattern and paleoproductivity.

4.1. Productivity indicators (Ba_{bio} flux, P_{org} flux): proxies for monsoonal intensity

The paleoproductivity during the period of study was determined by Ba_{bio}, and P_{org} fluxes. Ba is supplied to the seafloor mainly by two sources: (1) within the silicate lattice of river runoff sediments (continental input), and (2) in association with organic matter as barite. High Ba content was reported in the sediments underneath the high biological productivity areas of coastal upwelling and in the equatorial divergent zones (Goldberg and Arrhenius, 1958). Ba is used as a productivity proxy because of its refractory nature and high preservation potential/factor in sediments (Dymond et al., 1992; Gingele et al., 1999). Therefore, in order to estimate palaeoproductivity from the Ba content, it is necessary to distinguish the amount of Ba_{bio} from that of

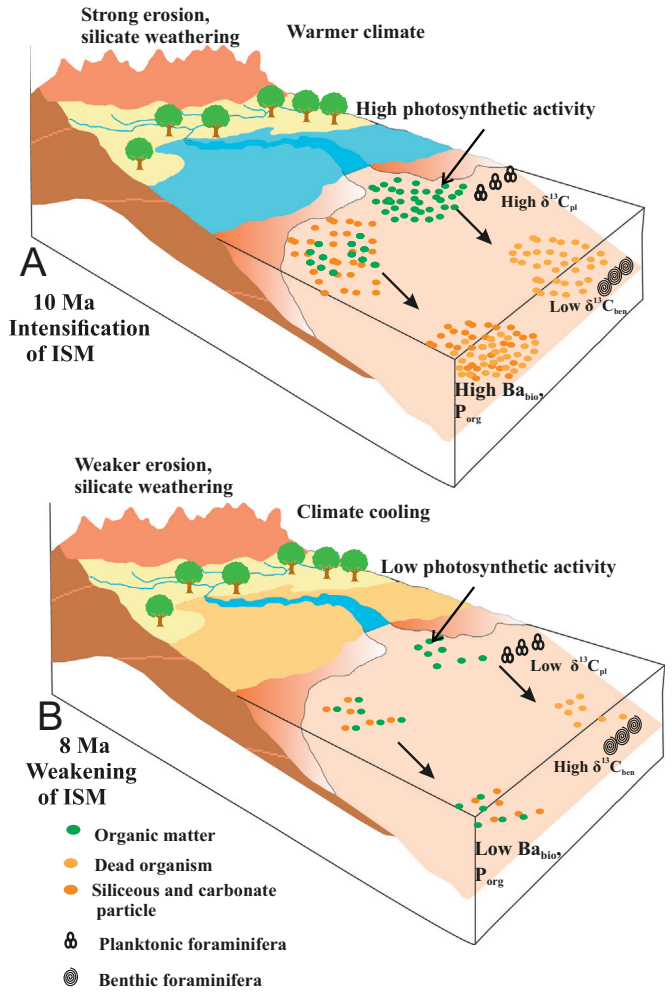

Fig. 3. Productivity model representing productivity variation in Bay of Bengal (BoB) in response to the Indian Summer Monsoon (ISM).

non-biogenic origin (Dymond et al., 1992; Gingele et al., 1999). Ba_{bio} was calculated by the amount of excess Ba (Ba_{excess}) (Schoepfer et al., 2015). Phosphorus (P) is structural and functional constituent of all organisms and serves as an essential nutrient in a marine ecosystem (Redfield, 1958; Schoepfer et al., 2015). In this study P_{org} instead of total P was used to obtain accurate biogenic P flux (Schoepfer et al., 2015). This calculation assumes all non-detrital P was derived from marine phytoplankton biomass. P_{org} flux serves as a good productivity proxy in Quaternary sediments of the Indian Ocean (Schenau et al., 2005).

The present Ba_{bio} concentration in the northern Indian Ocean sediments varies from a minimum value of 196 μg/g in the weak monsoon period to a maximum value of 1211 μg/g during stronger monsoon, which is almost equivalent to the value reported in the BoB during the period of this study (Balakrishnan Nair et al., 2005). The P_{org} concentrations in Quaternary sediments of northern Indian Ocean varies from 240 μg/g to 9095 μg/g between periods of weak and strengthened monsoon respectively (Shimmield and Mowbray, 1991). The highest value of P_{org} at our site is 13,180.4 μg/g which is higher than the maximum value of P_{org} reported in Quaternary sediments. High P_{org} and Ba_{bio} concentrations in middle Miocene sediments of ODP Site 758A relative to modern sediments of northern Indian Ocean indicate prevalence of monsoonal conditions during middle Miocene. The Ba_{bio} and P_{org} flux shows an increasing trend with highest value at ~10 Ma (Fig. 2D, F). The productivity proxies have been compared to stable oxygen isotope to its check glacial-interglacial variability. The P_{org}, Ba_{bio} and their fluxes exhibit high values during relatively warm period as compared to colder periods when compared to global and regional oxygen isotope data (grey region in Fig. 2A, B and C). The Ba_{bio} and P_{org} accumulation rates show a reasonably good correlation with another productivity proxy $\delta^{13}C_{pl}$-$\delta^{13}C_{ben}$ (Fig. 2E). The $\delta^{13}C$ difference between planktonic (pl) and benthic (ben) species ($\delta^{13}C_{pl}$-$\delta^{13}C_{ben}$) reflects periodic changes in surface-water productivity (Loubere, 1996; Schilman et al., 2001; Banerjee et al., 2017). High productivity enhances the removal of ^{12}C, resulting in increased $\delta^{13}C$ of surface water (Deuser et al., 1981; Hemleben et al., 1989). Simultaneously, the increased rate of raining organic matter and its oxidation at depths leads to $\delta^{13}C$ depletion of bottom waters (Loubere, 1996). Therefore, $\delta^{13}C_{pl}$-$\delta^{13}C_{ben}$ increases during high productivity event and decreases during the period of low productivity.

Primary productivity is governed by two factors: the availability of sunlight and availability of nutrients (Dash et al., 2011; Shukla et al., 2013). As BoB is situated in tropical region, where biological production is limited by the availability of nutrients rather than sunlight. The Site 758A receives river input of nutrients as well as above Site 758A, the southwest monsoon winds develop major divergences, inducing strong upwelling (Knox, 1987) and thus delivering nutrient rich subsurface water into the euphotic zone. Therefore, the mechanism by which nutrient is supplied to upper water of the BoB is strongly dependant on the ISM (Honjo and Weller, 1997; Woodward et al., 1999; Achary et al., 2014). The evolution of the ISM through time is still being debated. Numerous studies have highlighted the importance of the ISM on global climates (France-Lanord and Derry, 1994). The initiation or intensification of the ISM during the Miocene has been linked to the phased uplift of the Himalayas and Tibetan Plateau (Zhisheng et al., 2001), Antarctic glaciations, global climate changes (Gupta et al., 2004) and movement of the Inter Tropical Convergence Zone (ITCZ) with respect to the Indian Plate (Armstrong and Allen, 2011). Studies based on various proxies speculate the timing of monsoon initiation/intensification between 45 and 7 Ma (Quade et al., 1989; Ramstein et al., 1997; Clift and Gaedicke, 2002; Spicer et al., 2003; Gupta et al., 2004; Rowley and Currie, 2006; Clift et al., 2008), although a few records suggest major intensification of the ISM at roughly the same time as the "biogenic bloom" during the late Miocene (Chen et al., 2003; Gupta et al., 2004; Banerjee et al., 2017).

The stable isotope study at ODP Site 758A indicates initiation of the ISM at ~12 Ma and its intensification at ~10 Ma (Banerjee et al., 2017). The increase in primary productivity at ~12 Ma may be therefore linked to the initiation of the ISM. Intensification of the ISM may have increased weathering and erosion of rocks in the uplifted Himalayan region (Prell and Kutzbach, 1992). The weathered material was then transported to the BoB, thereby increasing nutrient flux and oceanic productivity (Filippelli, 1997) at ~10 Ma (Fig. 3A). Furthermore, the Himalayan Tibetan complex engendered land-sea thermal contrast and blocked the influence of the mid-westerlies, thus strengthening monsoonal winds and allowing more vigorous ocean upwelling and nutrient supply (Gupta et al., 2004; Gupta et al., 2015) (Fig. 3A). Increased upwelling and productivity enhanced organic matter production in the BoB. As the ISM intensified, it triggered rigorous physical and chemical erosion and organic carbon burial resulting in CO_2 drawdown that could have possibly contributed to advent of late Miocene cooling (LMC) at ~8 Ma (reverse greenhouse effect). However, this CO_2 drawdown was not solely caused by increased in paleoproductivity in Indian Ocean. The oceanic high productivity termed as 'biogenic bloom' occurred in a larger region (Indo Pacific divergence) than that affected by the monsoon (Berger et al., 1993; Dickens and Owen, 1994; Gupta et al., 2004). Researches concerning the biogenic bloom (Delaney and Filippelli, 1994; Dickens and Owen, 1994; 1996; Farrell et al., 1995a, 1995b; Rea and Snoeckx, 1995) indicates that increased primary productivity during this period was not only related to Himalayan uplift and upwelling in Indian Ocean but to a global-scale transfer of nutrients from other regions to Indo-Pacific divergence zones because of

accelerated deep water flow leading to further CO_2 drawdown and cooling in the late Miocene (Dickens and Owen, 1994). As there is a direct relationship between SST and modern summer monsoon, a decrease in SST resulted in weakening in the ISM intensity at ~10–8 Ma (Nicholls, 1995) (Fig. 3B). This period between ~10 and 8 is characterized by lower accumulation of Ba_{bio} and P_{org} (Fig. 2). Lower productivity in the Eastern Arabian Sea (EAS) and weak South Asian Monsoon (SAM) has been identified during the same time interval (Gupta et al., 2015; Tripathi et al., 2017). The productivity model in Figure 3 is a pictorial representation of the monsoonal variation from 10 to 8 Ma.

However, both the productivity proxies used in this study Ba_{bio} and P_{org} should not be used as a proxy for paleoproductivity in certain paleoenvironment. The barite formed is subjected to partial dissolution in under-saturated seawater, in reducing environment and in sulphate depletion zone (Von Breymann et al., 1990; Henkel et al., 2012). The efficacy of various processes retaining of P within the sediment also depends strongly on bottom-water oxygen concentrations. However, Ba_{bio} and P_{org} concentration proves to be a reliable paleoproductivity indicator in oxic and suboxic environments (Schmitz, 1987; Jumars et al., 1989; Gächter and Müller, 2003; Ingall et al., 2005). Therefore to find the validity of our productivity indicators we need to find out the bottom water oxygen conditions during the period of our study.

4.2. Trace and rare earth elements as proxies for depositional environments

The presence or absence of oxygen and H_2S determines the depositional conditions which vary between oxic, suboxic and anoxic environment in world oceans (Pattan et al., 2013). The redox conditions in sediments are often governed by biological productivity, supply of terrigenous input and upwelling intensity which in turn linked to strong monsoonal intensity (Gupta et al., 2004). Redox-sensitive trace metals are more soluble under oxidizing conditions and less soluble under reducing conditions which results in authigenic enrichment in sediments deposited under oxygen depleted environment. This behaviour makes U, V and to a lesser extent Cr useful paleoredox proxies (Tribovillard et al., 2006). In order to investigate changes in benthic redox conditions, we have calculated the U, V and Cr enrichment factors using Eq. (4). Enrichment factors > 3 indicate detectable authigenic enrichment while those exceeding 10 indicate substantial enrichment of an element (Algeo and Tribovillard, 2009; Pattan et al., 2013). Under oxic environment $U^{6+}$is present as Uranyl tricarbonate species which is highly soluble in water. The U^{6+} reduces to U^{4+} under reducing environment and becomes particle reactive and gets fixed onto sediments. Therefore, under anoxic conditions, U shows enrichment compared to the continental crust (Zheng et al., 2000; Pattan et al., 2017). The U concentrations in marine sediments have been proved to be an excellent paleoredox proxy to infer depositional environment (Dean et al., 1999; Algeo and Maynard, 2004; Algeo et al., 2012). It ranges between 0.2 and 1.9 μg/g (Fig. 4A) and thus are depleted compared to the upper continental crust (2.8 μg/g) (McLennan, 2001). Such depleted values of U indicate that the sediments were impinged by oxygenated waters. V is concentrated in sediments deposited under reducing conditions as it gets bounded to organic matter by the incorporation of V^{4+} into porphyrins (Shaw et al., 1990; Emerson and Huested, 1991). Under normal seawater conditions, the chromate anion is soluble, but under anoxic conditions, Cr(IV) is reduced to Cr(III), forming complexes and thus get exported to the sediments (Breit and Wanty, 1991; Algeo and Maynard, 2004). Cr is often transported to the sediment with the land-derived clastic fractions that have high Cr content, therefore giving false anoxic condition values (François, 1988; Brumsack, 1989; Hild and Brumsack, 1998). These complexities of Cr transport and enrichment limits its paleoenvironmental utility. However since the Cr_{Ef} remains < 3 in the entire core we have efficiently used it as a redox proxy in this study (Fig. 4D). The U_{EF} and V_{EF} also remains < 3 in the entire core indicating no authigenic enrichment and therefore points at oxic condition of deposition (Fig. 4B, C).

The glacial sediments in the northern Indian Ocean below a depth of about 2600 m report less oxygenated environment (Kallel et al., 1988; Sarkar et al., 1993). The most probable cause for such a reduction in the oxygen level of bottom water in the Indian Ocean was the reduction in the deep water formation during the Last glacial period (Sarkar et al., 1993). ODP Site 758A is located at a water depth of > 2900 m and oxic conditions throughout the study interval are a surprising result. The oxygenated bottom water conditions at Site 758A might be related to (i) EAIS expansion in the early middle Miocene that produced cold and oxygenated bottom waters (Woodruff and Douglas, 1981); (ii) Indian deep water formation which started with the final closure of the Middle Eastern Strait, about 16 Ma, and had been operating as a deep-water until North Atlantic deep water (NADW) started forming (Boersma, 1990); (iii) the production of oxygenated NADW and its export towards the Southern Ocean is also thought to have started in middle Miocene (Blanc et al., 1980; Thomas and Via, 2007; Banerjee et al., 2017). The inception of deep water formation during the middle Miocene must have resulted in well ventilated, oxygenated conditions at Site 758A irrespective of its depth. Moreover Site 758A lies outside the oxygen minimum zone that extends 5000 km in the southeast direction in the Indian Ocean (Dickens and Owen, 1999).

The PAAS-normalised REE patterns exhibit negative cerium (Ce/Ce*) anomaly (Fig. 4E). The Ce/Ce* ratio varies between 0.5 and 0.9, with an average value of 0.7 (Fig. 4E). Low Ce/Ce* (0.54–0.80) in the entire sediment core suggest anoxic-suboxic conditions and is not in agreement with the redox-sensitive element data (U, V and Cr) that indicates, the sediments were deposited in oxic conditions. Low Ce/Ce* (< 1) in the core could be due to high calcium carbonate content, where planktonic foraminifers have negative Ce anomaly in agreement with seawater REE pattern. Modern oxygenated seawater exhibits negative Ce anomaly. Several workers observed that stronger the negative Ce/Ce* anomaly, higher the carbonate content and vice versa (Wang et al., 1986; Nath et al., 1992).

4.3. Provenance of terrigenous sediments

Under modern conditions, terrigenous sediment fluxes from the Himalayan and Indo-Burman ranges are drained into the northeast Indian Ocean through major rivers like Ganges, Brahmaputra, Irrawaddy and Salween (Colin et al., 1999; Ahmad et al., 2005a). Since large volume of sediments in the BoB and the Andaman Sea are brought down by these river systems, they preserve imprints of the erosion and weathering history of Himalayan and Burman ranges (France-Lanord et al., 1993; Colin et al., 1999). Researchers have established a direct relationship between variations in the erosional products and changes in monsoonal precipitation over the Himalayan region during the late Quaternary (Singh and France-Lanord, 2002; Liu et al., 2005; Singh et al., 2008). The ODP Site 758A is within the influence of both the southwest and northeast monsoon currents (Schott and McCreary, 2001). The lithogenic sediments in the BoB derived from erosion of the Himalayan, Indo–Burman and Indian Peninsula regions help in understanding monsoon variations, weathering patterns and sediment provenance (Colin et al., 1999; Babu et al., 2010).

Increase in an overall K/Al ratio after ~12 Ma (Fig. 5C) may be related to higher contribution from the Himalayan river sediments, which are generally characterized by high K/Al ratios (Tripathy et al., 2014). Increase in Al weight percent at ~12 Ma also indicates higher input of terrestrial materials (Fig. 5D) (Goldberg and Arrhenius, 1958). The K content is generally high in illite and in some feldspar, and therefore the observed increase in K/Al at ~12 Ma may reflect higher contribution from these minerals (Colin et al., 1999; Singh et al., 2008). Uplift in the Himalayan-Tibetan region at 12 Ma (Crowley et al., 1998; Dettman et al., 2003; Anderson and Wellner, 2013, Tremblay et al., 2015) coupled with the ISM initiation might have increased erosion of source rocks (Chamley, 1989; Burbank et al., 1993; Molnar, 2001).

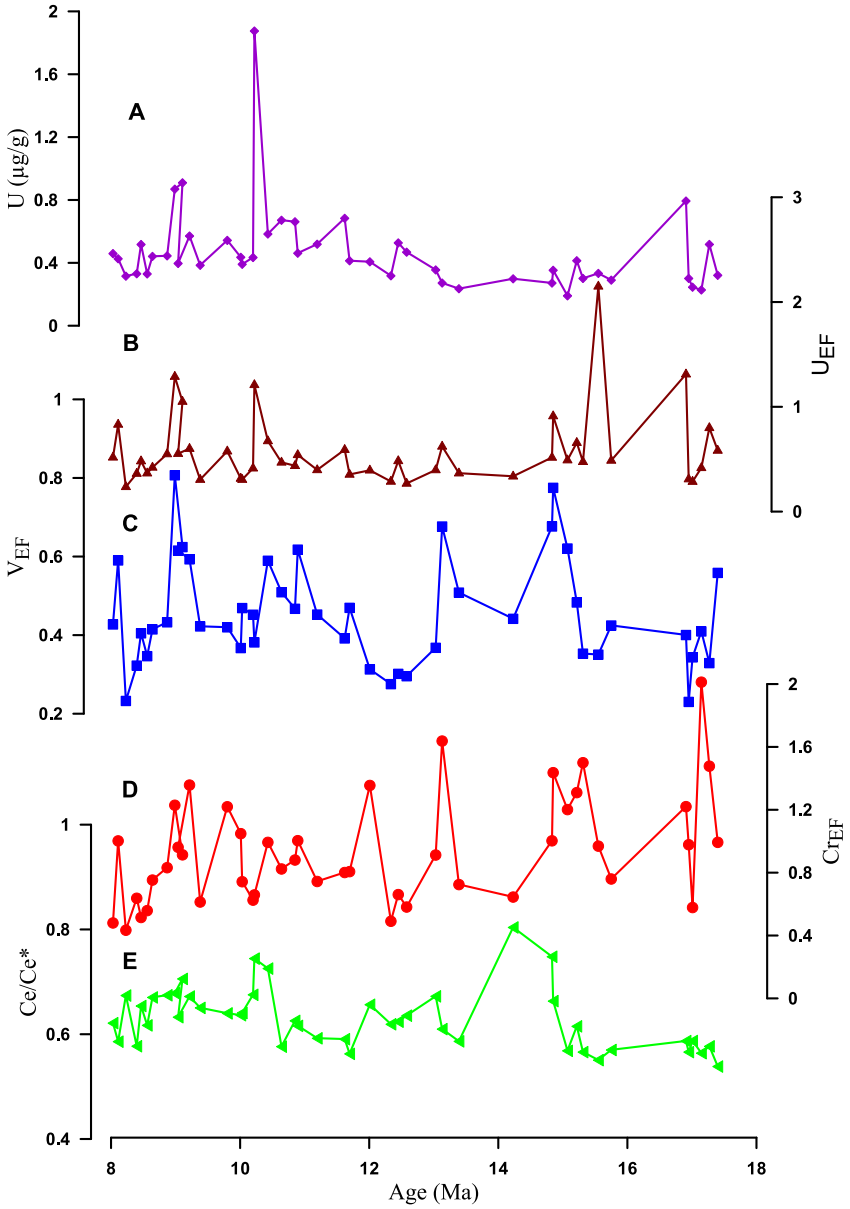

Fig. 4. Redox-sensitive elements as proxies for depositional environment. (A) U concentration in the sample, (B) U enrichment factor (U_{EF}), (C) V enrichment factor (V_{EF}), (D) Cr enrichment factor (Cr_{EF}) and (E) Ce/Ce* values.

Strong physical erosion inhibits chemical weathering and fosters the delivery of minerals like illite and feldspars, thereby increasing K/Al ratio from 12 to 8 Ma (Joussain et al., 2017). However, the source of low K/Al ratio before initiation of the ISM at ~12 Ma remains unknown. We have performed Sr and Nd isotope ratio measurements to unravel the link, if any, between the provenance of terrigenous flux at this site and the ISM.

Detrital particles in deep-sea cores are primarily the weathering products of continental rocks with a wide range of Sr and Nd isotope ratios. These particles are transported to the oceans by various means such as river, wind etc. Radiogenic isotopic compositions in deep sea sediments reflect signatures of their continental source and hence provide very useful information about their provenance (Goldstein et al., 1984; Revel et al., 1996). Studies on Nd isotopic compositions of Indian Ocean sediments suggest that the variations in $\varepsilon_{Nd}(0)$ are mainly due to changes in sediment source and transport pathway (Colin et al., 1999; Ahmad et al., 2005a). The active tectonic in Himalayan region, emerging monsoonal pattern and changing weathering intensity during Miocene may have influenced the sources and transport pathways of the sediments at ODP Site 758A. In the present day geographical set up, the Brahmaputra River originates in the Tibetan Himalaya and flows mainly through the Indus-Tsangpo Suture Zone, which is characterized by a lower $^{87}Sr/^{86}Sr$ (0.7037 to 0.7159) (France-Lanord et al., 1993; Singh and France-Lanord, 2002). Then it takes a south-western course in Shillong Plateau to join the Ganges. Brahmaputra water before joining Ganges at Goalpara gives $^{87}Sr/^{86}Sr$ ratio of 0.7192, which is significantly lower than the average value of Ganges water (0.720–0.780) (France-Lanord et al., 1993; Derry and France-Lanord, 1996; Colin et al., 1999).

The $^{87}Sr/^{86}Sr$ values range between 0.709 and 0.716, whereas $\varepsilon_{Nd}(0)$ ranges between −15.45 and −5.46, indicating a mixed source. The $^{87}Sr/^{86}Sr$ ratios and $\varepsilon_{Nd}(0)$ of sediments at ODP Site 717C in the western Bengal Fan (fed by Ganges-Brahmaputra river system) defines an average of ~0.741 and −16, respectively (France-Lanord et al., 1993) which is significantly different than the values reported at ODP Site 758A. Figure 6 shows the plot of $^{87}Sr/^{86}Sr$ ratios versus $\varepsilon_{Nd}(0)$ of

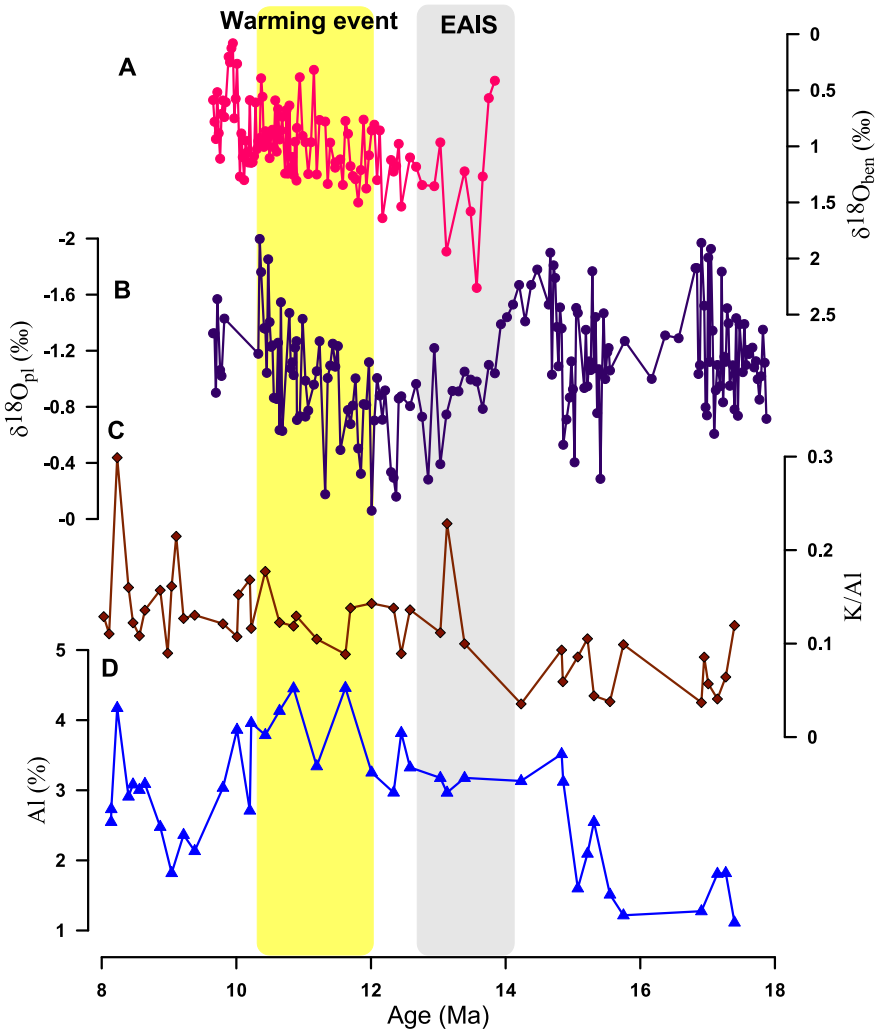

Fig. 5. Terrigenous input proxy in comparison with $\delta^{18}O_{ben}$ and $\delta^{18}O_{pl}$ of ODP Site 758A, (A) $\delta^{18}O_{ben}$ of ODP 758A (Banerjee et al., 2017), (B) $\delta^{18}O_{pl}$ of ODP 758A (Banerjee et al., 2017), (C) K/Al ratio, (D) Al (%). Grey shaded area represents cooling event (EAIS expansion) and the yellow shaded area represents warming event. (For interpretation of the references to colour in this figure legend, the reader is referred to the web version of this article.)

the samples, together with sediments from the Irrawaddy and Yarlung-Tsangpo Rivers, ODP Site 717C which is taken for Ganges-Brahmaputra (G-B) sediments (France-Lanord et al., 1993; Galy et al., 1996; Colin et al., 1999), Arakan coast sediments and fields of major Himalayan formation (Galy et al., 1996). The Sr and Nd isotopes of sediments from the ODP Site 717C lie in the range defined by the primary rocks from the High Himalaya Crystalline (HHC) (Bouquillon et al., 1990; France-Lanord et al., 1993; Derry and France-Lanord, 1996), whereas the sediments from ODP Site 758A fall in the field of the High Himalaya Sedimentary Series (HHSS) that reported to have characteristic values of $^{87}Sr/^{86}Sr$ (< 0.72) and $\varepsilon_{Nd}(0)$ (−12 to −4) (Derry and France-Lanord, 1996). This suggests that sediments deposited in the distal fan have a different source than those on the western Bengal Fan. Sediments at our study site are interpreted as derived by mixing from two potential isotopic endmembers. Irrawaddy River ($\varepsilon_{Nd}(0) = \sim -11$; $^{87}Sr/^{86}Sr = \sim 0.713$) and the second endmember has values similar to Arakan coast ($\varepsilon_{Nd}(0) = \sim -8$; $^{87}Sr/^{86}Sr = \sim 0.714$). This endmember is probably derived from detrital material generated by the erosion of the western part of the Indo-Burman ranges, along the Arakan coast (Fig. 1). Since the end members differ more in $\varepsilon_{Nd}(0)$ and less in $^{87}Sr/^{86}Sr$, we do not get a hyperbolic trend in Figure 9 despite of mixing of two sources (Colin et al., 1999). The low $^{87}Sr/^{86}Sr$ and less negative $\varepsilon_{Nd}(0)$ values in Irrawaddy sediments arise due to the weathering of Cretaceous and Oligocene sedimentary rocks, volcanic dykes and ophiolites from the Indo-Burmese ranges (Ahmad et al., 2005a). Hence, the middle Miocene sediments studied here show less influence of G-B river system and greater influence of Irrawaddy sediments. However, Brahmaputra in its upper reaches named Yarlung-Tsangpo, erodes Paleozoic to Eocene sedimentary rocks along with the plutonic and volcanic rocks of the suture that reported to exhibit low $^{87}Sr/^{86}Sr$ (0.711) and less radiogenic $\varepsilon_{Nd}(0)$ (−10.85) (Singh and France-Lanord, 2002; Yang et al., 2007).

In the modern scenario, the Andaman Sea receives sediments derived from the Tibetan highlands drained by the south flowing rivers, Irrawaddy and Salween (Curray et al., 1982). A possible conjecture could be that in the Miocene, the Yarlung-Tsangpo River was flowing into Irrawaddy River and finally reached the BoB, resulting in low $^{87}Sr/^{86}Sr$ values at our site. This paleodrainage system apparently eroded large amounts of detritus from the source region in the southern Tibet and transported to the Bengal Fan (Fig. 7A). Later with headward erosion of the Brahmaputra River this paleochannel may have been captured by Brahmaputra River to form the modern eastern Himalayan river system (Fig. 7B). Hence the sediments at ODP Site 758A during Miocene could be the products of Irrawaddy-Yarlung-Tsangpo drainage system that drained the Indus-Tsangpo Suture zone, southern Tibet, the eastern Himalayas and the Arakan coast. Although the exact age of this capture is unknown, the headward erosion of Brahmaputra River is often related to uplift of the Namche Barwa syntaxis, which took place

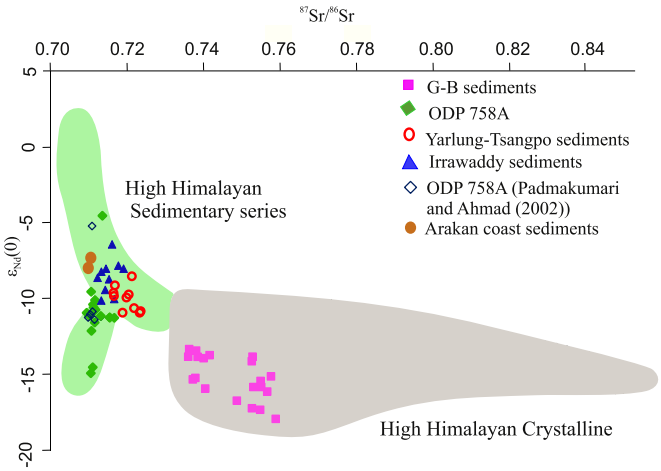

Fig. 6. The $^{87}Sr/^{86}Sr$ isotopic ratios versus $\varepsilon_{Nd}(0)$ for the middle Miocene sediments of ODP 758A. Sr and Nd isotopes of the ODP Site 717C sediments located in the distal portion of the Bengal Fan and all the major potential Himalayan sources are also included for comparison (Galy et al., 1996). Irrawaddy field is based on Irrawaddy River sample and sediment core data from the Andaman Sea, whereas Arakan coast is based on near coast sediments (Miriyala et al., 2017; Colin et al., 1999). Yarlung-Tsangpo field is based on Yarlung-Tsangpo River sediment samples (Yang et al., 2007). Previously analysed ODP Site 758A sediments are also included (Padmakumari and Ahmad, 2002).

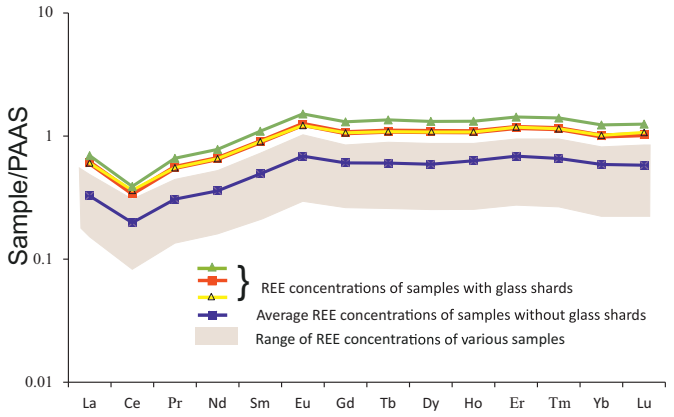

Fig. 8. Post Archean Australian Shale (PAAS) normalised REE pattern of sediments. The blue line represents average REE in sediments at ODP Site 758A without glass shards. Sediments with glass shards at ODP Site 758A are represented by green, yellow and red lines. The grey shaded area represents range of all sediment samples. (For interpretation of the references to colour in this figure legend, the reader is referred to the web version of this article.)

at 4 Ma (Burg et al., 1998; Clark et al., 2004; Liang et al., 2008). The Yarlung-Tsangpo sediments also lie in HHSS series and $^{87}Sr/^{86}Sr$ (0.7111) and $\varepsilon_{Nd}(0)$ (−10.85) values are almost identical to sediments of this study (Singh and France-Lanord, 2002; Yang et al., 2007). Moreover, the strong westerly current (derived from SW Monsoon winds) diverts most of the G-B sediment flux towards the abyssal plains away from the ridge which further reduces the influence of G-B sediments at our site (Ahmad et al., 2005a).

Our study indicates that the initiation of the ISM did not lead to any change in provenance of terrigenous flux at ODP Site 758A. The sediments were derived from the Himalayan region (HHSS) throughout the period of this study. However, prior to the initiation of the ISM and tectonic uplift of Tibetan Plateau, the sediments in BoB although derived from the highlands (Himalayan region), could have possibly underwent meteoric alteration in the lowland areas (Indo Gangetic Plains and Irrawaddy Basin) before depositing in the BoB, giving rise to low K/Al ratio (France-Lanord et al., 1993; Joussain et al., 2017).

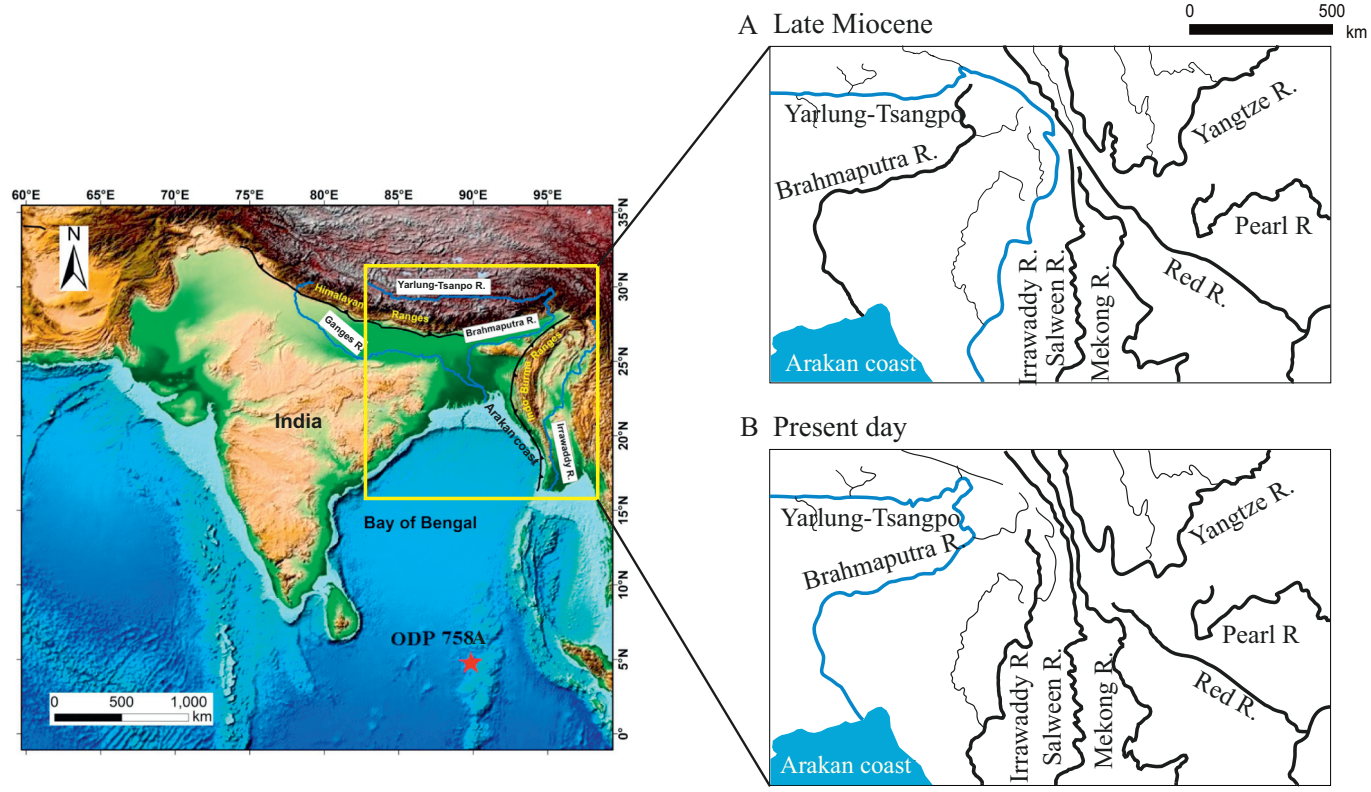

Fig. 7. (A) Representation of Yarlung-Tsangpo draining into Irrawaddy River (after Liang et al., 2008), (B) Modern Eastern Himalayan system, Yarlung-Tsangpo draining into Brahmaputra.

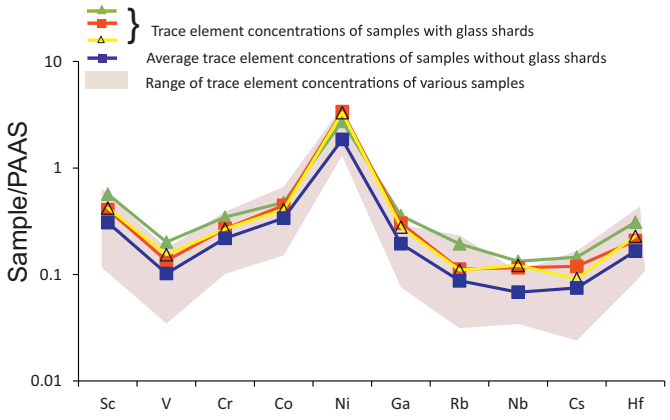

Fig. 9. PAAS normalised trace element patterns. Average trace element concentrations in marine sediments of ODP Site 758A showing absence of glass shards are represented with blue line. The green, yellow and red lines mark the average trace element concentrations of samples showing presence of glass shards. The grey shaded area represents range of all sediment samples. (For interpretation of the references to colour in this figure legend, the reader is referred to the web version of this article.)

5. Conclusions

Detailed geochemical and isotopic studies in sediments from ODP Site 758A in the southern BoB revealed paleoredox conditions, paleoproductivity and sediment provenance during the period of this study. Our study highlights the effect of initiation of the ISM on chemical characteristics of sediments. High P_{org} and Ba_{bio} in middle Miocene sediments indicate prevalence of monsoonal conditions during middle Miocene. Active tectonics and steep topography of the Himalayan region coupled with intense monsoon precipitation may have enhanced denudation rates in Himalayan-Burman ranges. The weathered material transported to the BoB coupled with strong upwelling in the region may have increased the nutrient flux and oceanic productivity at ~10 Ma.

Geochemical proxies suggest that the deep waters in southern BoB were well ventilated during the entire period of our study due to the formation of Antarctic deep waters, Indian deep waters and NADW, and its export towards the Southern Ocean in middle Miocene. Initiation of the ISM did not have any significant effect on provenance of sediments at ODP Site 758A, the sediments belong to High Himalayan sedimentary series throughout the period of study. However, prior to initiation of the ISM, the sediments underwent meteoric alteration in the lowlands before depositing in the BoB. The results indicate that the Yarlung-Tsangpo River was flowing into Irrawaddy River during Miocene, before draining into the BoB. Later headward erosion of the Brahmaputra River may have resulted in capture of Yarlung-Tsangpo to form the modern eastern Himalayan river system. The Miocene sediments of Site 758A could be products of Irrawaddy-Yarlung-Tsangpo drainage system that drained the Indus-Tsangpo Suture zone, southern Tibet, the eastern Himalayas and the Arakan coast. Initiation of the ISM at ~12 Ma probably resulted in changing signatures of productivity, erosion and weathering pattern. These signatures in the past reflects the emergence of modern like conditions during the middle Miocene.

Supplementary data to this article can be found online at https://doi.org/10.1016/j.palaeo.2018.10.022.

Acknowledgments

This research has been supported by 12th plan projects grant of CSIR-NGRI. The first author is thankful to the University Grant Commission (UGC) for grant under Junior Research Fellowship #F.2/2002 (SA-I). We are also thankful to IODP repository Kochi, Japan for providing samples and to Dr. Lallan Gupta, Curator IODP repository, Kochi, Japan for his help and support. We are thankful to Mr. Waseem Raza, Mrs. G. Suseela, Dr. Tabish Raza, Mr. Netramani Sagar and Dr. S.S. Sawant for their help during the course of this study. We are grateful to Dr. V.M Tiwari, Director, CSIR-NGRI for facilities, encouragement and permission to publish this paper. We express our thanks to Prof. Thomas Algeo, two anonymous reviewers, Dr V. Purnachandra Rao and Dr B. Nagender Nath for their constructive comments to improve the manuscript.

References

Achary, M.S., Panigrahi, S., Satpathy, K.K., Sahu, G., Mohanty, A.K., Selvanayagam, M., Panigrahy, R.C., 2014. Nutrient dynamics and seasonal variation of phytoplankton assemblages in the coastal waters of southwest Bay of Bengal. Environ. Monit. Assess. 186 (9), 5681–5695.

Ahmad, S.M., Babu, G.A., Padmakumari, V.M., Dayal, A.M., Sukhija, B.S., Nagabhushanam, P., 2005a. Sr, Nd isotopic evidence of terrigenous flux variations in the Bay of Bengal: implications of monsoons during the last ~34,000 years. Geophys. Res. Lett. 32 (22).

Ahmad, S.M., Dayal, A.M., Padmakumari, V.M., Anil Babu, G., Gopalan, K., 2005b. Changes in seawater $^{87}Sr/^{86}Sr$ curve during early Miocene to early late Miocene: Implications for ODP 758 record. J. Geol. Soc. India 65, 147–157.

Algeo, T.J., Maynard, J.B., 2004. Trace-element behavior and redox facies in core shales of Upper Pennsylvanian Kansas-type cyclothems. Chem. Geol. 206 (3), 289–318.

Algeo, T.J., Tribovillard, N., 2009. Environmental analysis of paleoceanographic systems based on molybdenum–uranium covariation. Chem. Geol. 268 (3), 211–225.

Algeo, T.J., Morford, J., Cruse, A., 2012. Reprint of: New applications of trace metals as proxies in marine paleoenvironments. Chem. Geol. 324–325, 160–164.

Anderson, J.B., Wellner, J.S. (Eds.), 2013. Tectonic, Climatic, and Cryospheric Evolution of the Antarctic Peninsula. vol 63 John Wiley & Sons.

Armstrong, H.A., Allen, M.B., 2011. Shifts in the intertropical convergence zone, Himalayan exhumation and late Cenozoic climate. Geology 39, 11–14.

Babu, C.P., Pattan, J.N., Dutta, K., Basavaiah, N., Prasad, G.R., Ray, D.K., Govil, P., 2010. Shift in detrital sedimentation in the eastern Bay of Bengal during the late Quaternary. J. Earth Syst. Sci. 119 (3), 285–295.

Balakrishnan Nair, T.M., Ittekkot, V., Shankar, R., Guptha, M.V.S., 2005. Settling barium fluxes in the Arabian sea: critical evaluation of relationship with export production. Deep-Sea Res. II Top. Stud. Oceanogr. 52, 1930–1946.

Banerjee, B., Ahmad, S.M., Raza, W., Raza, T., 2017. Paleoceanographic changes in the Northeast Indian Ocean during middle Miocene inferred from carbon and oxygen isotopes of foraminiferal fossil shells. Palaeogeogr. Palaeoclimatol. Palaeoecol. 466, 166–173.

Bau, M., Dulski, P., 1996. Distribution of yttrium and rare-earth elements in the Penge and Kuruman iron-formations, Transvaal Super group, South Africa. Precambrian Res. 79, 37–55.

Berger, W.H., Leckie, R.M., Janecek, T.R., Stax, R., Takayama, T., 1993. Neogene carbonate sedimentation on Ontong-Java-Plateau highlights and open questions. Proc. ODP Sci. Results 130, 711–744.

Bird, M.I., Robinson, R.A.J., Oo, N.W., Aye, M.M., Lu, X.X., Higgitt, D.L., Swe, A., Tun, T., Win, S.L., Aye, K.S., Win, K.M.M., 2008. A preliminary estimate of organic carbon transport by the Ayeyarwady (Irrawaddy) and Thanlwin (Salween) Rivers of Myanmar. Quat. Int. 186 (1), 113–122.

Blanc, P.L., Rabussier, D., Vergnaud-Grazzini, C., Duplessy, J.C., 1980. North Atlantic deep water formed by the later middle Miocene. Nature 283 (5747), 553–555.

Boersma, A., 1990. Late Oligocene to late Pliocene benthic foraminifers from depth traverses in the central Indian Ocean. Proc. Ocean Drill. Program Sci. Results 115, 315–379.

Bouquillon, A., France-Lanord, C., Michard, A., Tiercelin, J.J., 1990. Sedimentology and isotopic chemistry of the bengal fan sediments: the denudation of the Himalaya. Proc. Ocean Drill. Program Sci. Results 116, 43–58.

Breit, G.N., Wanty, R.B., 1991. Vanadium accumulation in carbonaceous rocks: a review of geochemical controls during deposition and diagenesis. Chem. Geol. 91 (2), 83–97.

Brumsack, H.J., 1989. Geochemistry of recent TOC-rich sediments from the Gulf of California and the Black Sea. Geol. Rundsch. 78, 851–882.

Burbank, D.W., Derry, L.A., France-Lanord, C., 1993. Reduced Himalayan sediment production 8 Myr ago despite an intensified monsoon. Nature 364 (6432), 48–50.

Burg, J.P., Nievergelt, P., Oberli, F., Seward, D., Davy, P., Maurin, J.C., Diao, Z., Meier, M., 1998. The Nambshe-Barwa syntaxis: evidence for exhumation related to compressional crustal folding. J. Asian Earth Sci. 16, 239–252.

Calvert, S.E., Pedersen, T.F., 1993. Geochemistry of recent oxic and anoxic marine sediments: implications for the geological record. Mar. Geol. 113 (1–2), 67–88.

Chakrapani, G.J., Saini, R., 2009. Temporal and spatial variations in water discharge and sediment load in the Alaknanda and Bhagirathi Rivers in Himalaya, India. J. Asian Earth Sci. 35, 545–553.

Chamley, H., 1989. Clay formation through weathering. In: Clay Sedimentology. Springer, Berlin, Heidelberg, pp. 21–50.

Chen, M., Wang, R., Yang, L., Han, J., Lu, J., 2003. Development of east Asian summer monsoon environments in the late Miocene: radiolarian evidence from Site 1143 of ODP Leg 184. Mar. Geol. 201 (1), 169–177.

Clark, M.K., Schoenbohm, L.M., Royden, L.H., Whipple, K.X., Burchfiel, B.C., Zhang, X., Tang, W., Wang, E., Chen, L., 2004. Surface uplift, tectonics, and erosion of eastern Tibet from large-scale drainage patterns. Tectonics 23 (1).

Clift, P., Gaedicke, C., 2002. Accelerated mass flux to the Arabian Sea during the middle to late Miocene. Geology 30, 207–210.
Clift, P.D., Hodges, K.V., Heslop, D., Hanningan, R., Van Long, H., Calves, G., 2008. Correlation of Himalayan exhumation rates and Asian monsoon intensity. Nat. Geosci. 1, 875–880.
Colin, C., Turpin, L., Bertaux, J., Desprairies, A., Kissel, C., 1999. Erosional history of the Himalayan and Burman ranges during the last two glacial–interglacial cycles. Earth Planet. Sci. Lett. 171 (4), 647–660.
Crowley, S.F., Stow, D.A., Croudace, I.W., 1998. Mineralogy and geochemistry of Bay of Bengal deep-sea fan sediments, ODP Leg 116: evidence for an Indian subcontinent contribution to distal fan sedimentation. Geol. Soc. Lond., Spec. Publ. 131 (1), 151–176.
Curray, J.R., 1994. Sediment volume and mass beneath the Bay of Bengal. Earth Planet. Sci. Lett. 125, 371–383.
Curray, J.R., Emmel, F.J., Moore, D.G., Raitt, R.W., 1982. Struscture, tectonics, and geological history of the northeastern Indian Ocean. In: Nairn, A.E.M., Stehli, F.G. (Eds.), The Ocean Basins and Margins. Springer, US, pp. 399–450.
Dalai, T.K., Krishnaswami, S., Sarin, M.M., 2002. Major ion chemistry in the headwaters of the Yamuna river system: chemical weathering, its temperature dependence and CO_2 consumption in the Himalaya. Geochim. Cosmochim. Acta 66 (19), 3397–3416.
Das, A., Krishnaswami, S., Sarin, M.M., Pande, K., 2005. Chemical weathering in the Krishna Basin and Western Ghats of the Deccan Traps, India: rates of basalt weathering and their controls. Geochim. Cosmochim. Acta 2067–2084.
Dash, S., Patra, A.K., Adhikary, S., 2011. Primary Productivity of Kharasrota River (India). J. Ecophysiol. Occup. Health 11, 219–225.
Dean, W.E., Piper, D.Z., Peterson, L.C., 1999. Molybdenum accumulation in Cariaco basin sediment over the past 24 kyr: a record of water-column anoxia and climate. Geology 27 (6), 507–510.
Dehairs, F., Chesselet, R., Jedwab, J., 1980. Discrete suspended particles of barite and the barium cycle in the open ocean. Earth Planet. Sci. Lett. 49, 528–550.
Delaney, M.L., 1998. Phosphorus accumulation in marine sediments and the oceanic phosphorus cycle. Glob. Biogeochem. Cycles 12, 563–572.
Delaney, M.L., Filippelli, G.M., 1994. An apparent contradiction in the role of phosphorus in Cenozoic chemical mass balances for the world ocean. Paleoceanography 9, 513–527.
Derry, L.A., France-Lanord, C., 1996. Neogene Himalayan weathering history and river $^{87}Sr/^{86}Sr$: Impact on the marine Sr record. Earth Planet. Sci. Lett. 142, 59–74.
Dettman, D.L., Fang, X., Garzione, C.N., Li, J., 2003. Uplift-driven climate change at 12 Ma: a long $\delta^{18}O$ record from the NE margin of the Tibetan plateau. Earth Planet. Sci. Lett. 214 (1), 267–277.
Deuser, W.G., Ross, E.H., Hemleben, C., Spindler, M., 1981. Seasonal changes in species composition numbers, mass, size and isotopic composition of planktonic foraminifera settling into the deep Sargasso Sea. Palaeogeogr. Palaeoclimatol. Palaeoecol. 33, 103–127.
Dickens, G.R., Owen, R.M., 1994. Late Miocene-early Pliocene manganese redirection in the central Indian Ocean: expansion of the intermediate water oxygen minimum zone. Paleoceanography 9 (1), 169–181.
Dickens, G.R., Owen, R.M., 1996. Sediment geochemical evidence for an early-middle Gilbert (early Pliocene) productivity peak in the North Pacific Red Clay Province. Mar. Micropaleontol. 27 (1-4), 107–120.
Dickens, G.R., Owen, R.M., 1999. The latest Miocene–early Pliocene biogenic bloom: a revised Indian Ocean perspective. Mar. Geol. 161 (1), 75–91.
Dymond, J., Suess, E., Lyle, M., 1992. Barium in deep-sea sediment: a geochemical proxy for paleoproductivity. Paleoceanography 7 (2), 163–181.
Emerson, S.R., Huested, S.S., 1991. Ocean anoxia and the concentrations of molybdenum and vanadium in seawater. Mar. Chem. 34, 177–196.
Farrell, J.W., Janecek, T.R., 1991. Late Neogene paleoceanography and paleoclimatology of the Northeast Indian Ocean (Site 758). Proc. Ocean Drill. Program Sci. Results 121, 297–355 Texas.
Farrell, J.W., Clemens, S.C., Gromet, L.P., 1995a. Improved chronostratigraphic reference curve of late Neogene seawater $^{87}Sr/^{86}$ Sr. Geology 23, 403–406.
Farrell, J.W., Raffi, I., Janecek, T.R., Murray, D.W., Levitan, M., Dadey, K.A., Emeis, K.-C., Lyle, M., Flores, J.-A., Hovan, S., 1995b. Late Neogene sedimentation patterns in the eastern equatorial Pacific Ocean. Proc. Ocean Drill. Program Sci. Results 138, 717–756.
Filippelli, G.M., 1997. Intensification of the Asian monsoon and a chemical weathering event in the late Miocene–early Pliocene: implications for late Neogene climate change. Geology 25 (1), 27–30.
Flower, B.P., Kennett, J.P., 1993. Middle Miocene ocean-climate transition: High-resolution oxygen and carbon isotopic records from deep sea drilling project site 588A, southwest Pacific. Paleoceanography 8 (6), 811–843.
Flower, B.P., Kennett, J.P., 1995. Middle Miocene deepwater paleoceanography in the southwest Pacific: relations with East Antarctic Ice Sheet development. Paleoceanography 10 (6), 1095–1112.
France-Lanord, C., Derry, L.A., 1994. $\delta^{13}C$ of organic carbon in the Bengal Fan: source evolution and transport of C_3 and C_4 plant carbon to marine sediments. Geochim. Cosmochim. Acta 58 (21), 4809–4814.
France-Lanord, C., Derry, L., Michard, A., 1993. Evolution of the Himalaya since Miocene time: isotopic and sedimentological evidence from the Bengal Fan. Geol. Soc. Lond., Spec. Publ. 74 (1), 603–621.
François, R., 1988. A study on the regulation of the concentrations of some trace metals (Rb, Sr, Zn, Pb, Cu, V, Cr, Ni, Mn and Mo) in Saanich Inlet sediments, British Columbia, Canada. Mar. Geol. 83, 285–308.
Gächter, R., Müller, B., 2003. Why the phosphorus retention of lakes does not necessarily depend on the oxygen supply to their sediment surface. Limnol. Oceanogr. 48 (2), 929–933.
Galy, A., France-Lanord, C., Derry, L.A., 1996. The Late Oligocene-Early Miocene Himalayan belt constraints deduced from isotopic compositions of Early Miocene turbidites in the Bengal Fan. Tectonophysics 260 (1), 109–118.
Gingele, F.X., Zabel, M., Kasten, S., Bonn, W.J., Nurnberg, C.C., 1999. Biogenic barium as a proxy for paleoproductivity: methods and limitations of application. In: Fischer, G., Wefer, G. (Eds.), Uses of Proxies in Paleoceanography: Examples from the South Atlantic. Springer, Berlin, pp. 345–364.
Goldberg, E.D., Arrhenius, G., 1958. Chemistry of Pacific pelagic sediments. Geochim. Cosmochim. Acta 13, 153–212.
Goldstein, S.L., O'Nions, R.K., Hamilton, P.J., 1984. A Sm-Nd isotopic study of atmospheric dusts and particulates from major river systems. Earth Planet. Sci. Lett. 70 (2), 221–236.
Gupta, A.K., Singh, R.K., Joseph, S., Thomas, E., 2004. Indian Ocean high-productivity event (10–8 Ma): Linked to global cooling or to the initiation of the Indian monsoons? Geology 32 (9), 753–756.
Gupta, A.K., Yuvaraja, A., Prakasam, M., Clemens, S.C., Velu, A., 2015. Evolution of the south Asian monsoon wind system since the late Middle Miocene. Palaeogeogr. Palaeoclimatol. Palaeoecol. 438, 160–167.
Hemleben, C., Spindler, M., Anderson, O.R., 1989. Modern Planktonic Foraminifera. Springer Science & business media.
Henkel, S., Mogollón, J.M., Nöthen, K., Franke, C., Bogus, K., Robin, E., Bahr, A., Blumenberg, M., Pape, T., Seifert, R., März, C., 2012. Diagenetic barium cycling in Black Sea sediments–a case study for anoxic marine environments. Geochim. Cosmochim. Acta 88, 88–105.
Hild, E., Brumsack, H.J., 1998. Major and minor element geochemistry of Lower Aptian sediments from the NW German Basin (core Hoheneggelsen KB 40). Cretac. Res. 19, 615–633.
Hodell, D.A., Mueller, P.A., Garrido, J.R., 1991. Variations in the strontium isotopic composition of seawater during the Neogene. Geology 19, 24–27.
Holbourn, A., Kuhnt, W., Schulz, M., Erlenkeuser, H., 2005. Impacts of orbital forcing and atmospheric carbon dioxide on Miocene ice-sheet expansion. Nature 438 (7067), 483–487.
Holbourn, A., Kuhnt, W., Schulz, M., Flores, J.A., Andersen, N., 2007. Orbitally-paced climate evolution during the middle Miocene "Monterey" carbon-isotope excursion. Earth Planet. Sci. Lett. 261 (3), 534–550.
Holbourn, A., Kuhnt, W., Clemens, S., Prell, W., Andersen, N., 2013. Middle to late Miocene stepwise climate cooling: evidence from a high resolution deep water isotope curve spanning 8 million years. Paleoceanography 28, 688–699.
Holbourn, A., Kuhnt, W., Lyle, M., Schneider, L., Romero, O., Andersen, N., 2014. Middle Miocene climate cooling linked to intensification of eastern equatorial Pacific upwelling. Geology 42 (1), 19–22.
Holbourn, A., Kuhnt, W., Kochhann, K.G.D., Andersen, N., Meier, K.J.S., 2015. Global perturbation of the carbon cycle at the onset of the Miocene Climatic Optimum. Geology 43, 123–126.
Honjo, S., Weller, R.A., 1997. Monsoon winds and carbon cycles in the Arabian Sea. In: Oceanus-woods Hole Mass. 40. pp. 24–28.
Huh, Y., 2010. Estimation of atmospheric CO_2 uptake by silicate weathering in the Himalayas and the Tibetan Plateau: a review of existing fluvial geochemical data. Geol. Soc. Lond., Spec. Publ. 342 (1), 129–151.
Ingall, E., Kolowith, L., Lyons, T., Hurtgen, M., 2005. Sediment carbon, nitrogen and phosphorus cycling in an anoxic fjord, Effingham Inlet, British Columbia. Am. J. Sci. 305 (3), 240–258.
Jia, G., Peng, P.A., Zhao, Q., Jian, Z., 2003. Changes in terrestrial ecosystem since 30 Ma in East Asia: stable isotope evidence from black carbon in the South China Sea. Geology 31 (12), 1093–1096.
Jones, M.T., Gislason, S.R., 2008. Rapid releases of metal salts and nutrients following the deposition of volcanic ash into aqueous environments. Geochim. Cosmochim. Acta 72 (15), 3661–3680.
Joussain, R., Liu, Z., Colin, C., Duchamp-Alphonse, S., Yu, Z., Moréno, E., Fournier, L., Zaragosi, S., Dapoigny, A., Meynadier, L., Bassinot, F., 2017. Link between Indian monsoon rainfall and physical erosion in the Himalayan system during the Holocene. Geochem. Geophys. Geosyst. 18 (9), 3452–3469.
Jumars, P.A., Altenbach, A.V., De Lange, G.J., Emerson, S.R., Hargrave, B.T., Muller, P.J., Prahl, F.G., Reimers, C.E., Steiger, T., Suess, E., 1989. Transformation of seafloor-arriving fluxes into the sedimentary record. In: Berger, W.H., Smetacek, V.S., Wefer, G. (Eds.), Productivity of the Ocean: Present and Past. John Wiley and Sons, Chichester, UK, pp. 291–301.
Kallel, N., Labeyrie, L.D., Juillet-Leclerc, A., Duplessy, J.C., 1988. A deep hydrological front between intermediate and deep-wafpr, masses in the glacial Indian Ocean. Nature 333 (6174), 651–655.
Kessarkar, P.M., Rao, V.P., Ahmad, S.M., Patil, S.K., Kumar, A.A., Babu, G.A., Rajan, R.S., 2005. Changing sedimentary environment during the Late Quaternary: sedimentological and isotopic evidence from the distal Bengal Fan. Deep-Sea Res. I Oceanogr. Res. Pap. 52 (9), 1591–1615.
Klootwijk, C.T., Gee, J.S., Peirce, J.W., Smith, G.M., 1992. Neogene evolution of the Himalayan-Tibetan region: constraints from ODP Site 758, northern Ninetyeast Ridge; bearing on climatic change. Palaeogeogr. Palaeoclimatol. Palaeoecol. 95 (1–2), 95–110.
Knox, R.A., 1987. The Indian Ocean: interaction with the monsoons. In: Fein, J.S., Stephens, P.L. (Eds.), Monsoons. John Wiley, New York, pp. 365–397.
Kolla, V., Rao, N.M., 1990. Sedimentary sources in the surface and near-surface sediments of the Bay of Bengal. Geo-Mar. Lett. 10, 129–136.
Krishna, A.K., Govil, P.K., 2007. Soil contamination due to heavy metals from an industrial area of Surat, Gujarat, Western India. Environ. Monit. Assess. 124 (1), 263–275.
Liang, Y.H., Chung, S.L., Liu, D., Xu, Y., Wu, F.Y., Yang, J.H., Wang, Y., Lo, C.H., 2008.

Detrital zircon evidence from Burma for reorganization of the eastern Himalayan river system. Am. J. Sci. 308 (4), 618–638.
Licht, A., Van Cappelle, M., Abels, H.A., Ladant, J.B., Trabucho-Alexandre, J., France-Lanord, C., Donnadieu, Y., Vandenberghe, J., Rigaudier, T., Lécuyer, C., Terry Jr., D., 2014. Asian monsoons in a late Eocene greenhouse world. Nature 513 (7519), 501–506.
Liu, Z., Colin, C., Trentesaux, A., Siani, G., Frank, N., Blamart, D., Farid, S., 2005. Late Quaternary climatic control on erosion and weathering in the eastern Tibetan Plateau and the Mekong Basin. Quat. Res. 63 (3), 316–328.
Loubere, P., 1996. The surface ocean productivity and bottom water oxygen signals in deep water benthic foraminiferal assemblages. Mar. Micropaleontol. 28, 247–261.
McLennan, S.M., 2001. Relationships between the trace element composition of sedimentary rocks and upper continental crust. Geochem. Geophys. Geosyst. 2 (4).
Miller, K.G., Wright, J.D., Fairbanks, R.G., 1991. Unlocking the ice house: Oligocene-Miocene oxygen isotopes, ecstasy and margin erosion. J. Geophys. Res. 96, 6829–6848.
Miriyala, P., Sukumaran, N.P., Nath, B.N., Ramamurty, P.B., Sijinkumar, A.V., Vijayagopal, B., Ramaswamy, V., Sebastian, T., 2017. Increased chemical weathering during the deglacial to mid-Holocene summer monsoon intensification. Sci. Rep. 7, 44310.
Molnar, P., 2001. Climate change, flooding in arid environments, and erosion rates. Geology 29 (12), 1071–1074.
Nath, B.N., Roelandts, I., Sudhakar, M., Pluger, W., 1992. Rare earth element patterns of the central Indian basin sediment related to their lithology. Geophys. Res. Lett. 19, 1197–2000.
Nicholls, N., 1995. All-India summer monsoon rainfall and sea surface temperatures around northern Australia and Indonesia. J. Clim. 8, 1463–1467.
Östlund, H.G., Oleson, R., Brescher, R., 1980. GEOSECS Indian Ocean Radiocarbon and Tritium Results (Miami). In: Rosenstiel School of Marine and Atmospheric Science, University of Miami.
Padmakumari, V.M., Ahmad, S.M., 2002. Provenance and nature of Miocene clastic sediments at ODP Site 758 A in Northeast Indian Ocean: Sr and Nd isotopic studies. J. Appl. Geochem. 4, 254–262.
Pattan, J.N., Mir, I.A., Parthiban, G., Karapurkar, S.G., Matta, V.M., Naidu, P.D., Naqvi, S.W.A., 2013. Coupling between suboxic condition in sediments of the western Bay of Bengal and southwest monsoon intensification: a geochemical study. Chem. Geol. 343, 55–66.
Pattan, J.N., Parthiban, G., Garg, A., Moraes, N.C., 2017. Intense reducing conditions during the last deglaciation and Heinrich events (H1, H2, H3) in sediments from the oxygen minimum zone off Goa, eastern Arabian Sea. Mar. Pet. Geol. 84, 243–256.
Peirce, J., Weissel, J., Party, S.S., 1989. Ninetyeast ridge summary. In: Proceedings of Ocean Drilling Program, Initial Reports. 121. pp. 517–537.
Ponomareva, V., Portnyagin, M., Davies, S.M., 2015. Tephra without borders: far-reaching clues into past explosive eruptions. Front. Earth Sci. 3, 83.
Prell, W.L., Kutzbach, J.E., 1992. Sensitivity of the Indian monsoon to forcing parameters and implications for its evolution. Nature 360, 647–651.
Quade, J., Cerling, T.E., Bowman, J.R., 1989. Development of Asian monsoon revealed by marked ecological shift during the latest Miocene in northern Pakistan. Nature 342, 163–166.
Rahaman, W., Singh, S.K., Sinha, R., Tandon, S.K., 2009. Climate control on erosion distribution over the Himalaya during the past ~100 ka. Geology 37 (6), 559–562.
Ramaswamy, V., Nair, R.R., 1994. Fluxes of material in the Arabian Sea and Bay of Bengal—sediment trap studies. Proc. - Indian Acad. Sci. Earth Planet. Sci. 103 (2), 189–210.
Ramstein, G., Fluteau, F., Besse, J., Joussaume, S., 1997. Effect of orogeny, plate motion and land-sea distribution on Eurasian climate change over the past 30 million years. Nature 386, 788–795.
Rawson, H., Naranjo, J.A., Smith, V.C., Fontijn, K., Pyle, D.M., Mather, T.A., Moreno, H., 2015. The frequency and magnitude of post-glacial explosive eruptions at Volcán Mocho-Choshuenco, southern Chile. J. Volcanol. Geotherm. Res. 299, 103–129.
Rea, D.K., Snoeckx, H., 1995. Sediment fluxes in the Gulf of Alaska: paleoceanographic record from Site 887 on the Patton– Murray Seamount Platform. Proc. Ocean Drill. Program Sci. Results 145, 247–256.
Redfield, A.C., 1958. The biological control of chemical factors in the environment. Am. Sci. 46 (3), 205–221.
Reitz, A., Pfeifer, K., De Lange, G.J., Klump, J., 2004. Biogenic barium and the detrital Ba/Al ratio: a comparison of their direct and indirect determination. Mar. Geol. 204 (3–4), 289–300.
Revel, M., Cremer, M., Grousset, F.E., Labeyrie, L., 1996. Grain-size and Sr-Nd isotopes as tracer of paleo-bottom current strength, Northeast Atlantic Ocean. Mar. Geol. 131 (3–4), 233–249.
Rowley, D.B., Currie, B.S., 2006. Palaeo-altimetry of the late Eocene to Miocene Lunpola basin, central Tibet. Nature 439, 677–681.
Sarkar, A., Bhattacharya, S.K., Sarin, M.M., 1993. Geochemical evidence for anoxic deep water in the Arabian Sea during the last glaciation. Geochim. Cosmochim. Acta 57 (5), 1009–1016.
Satyanarayanan, M., Balaram, V., Sawant, S.S., Subramanyam, K.S.V., Krishna, G.V., 2014. High precision multielement analysis on geological samples by HR-ICP-MS. In: 28th ISMAS Symposium Cum Workshop on Mass Spectrometry. Indian Society for Mass Spectrometry, Mumbai, pp. 181–184.
Schenau, S.J., Reichart, G.J., De Lange, G.J., 2005. Phosphorus burial as a function of paleoproductivity and redox conditions in Arabian Sea sediments. Geochim. Cosmochim. Acta 69 (4), 919–931.
Schilman, B., Labin, A.A., Mathew, M.R., Laberie, L., Paterne, M., Luz, B., 2001. Long and short-term carbon fluctuations in the Eastern Mediterranean during the late Holocene. Geology 29, 1099–1102.
Schmitz, B., 1987. Barium, equatorial high productivity, and the northward wandering of the Indian continent. Paleoceanography 2 (1), 63–77.
Schneider, R.R., Price, B., Müller, P.J., Kroon, D., Alexander, I., 1997. Monsoon related variations in Zaire (Congo) sediment load and influence of fluvial silicate supply on marine productivity in the east equatorial Atlantic during the last 200,000 years. Paleoceanography 12, 463–481.
Schoepfer, S.D., Shen, J., Wei, H., Tyson, R.V., Ingall, E., Algeo, T.J., 2015. Total organic carbon, organic phosphorus, and biogenic barium fluxes as proxies for paleomarine productivity. Earth Sci. Rev. 149, 23–52.
Schott, F.A., McCreary, J.P., 2001. The monsoon circulation of the Indian Ocean. Prog. Oceanogr. 51 (1), 1–123.
Shaw, T.J., Geiskes, J.M., Jahnke, R.A., 1990. Early diagenesis in differing depositional environments: the response of transition metals in pore water. Geochim. Cosmochim. Acta 54, 1233–1246.
Shimmield, G.B., Mowbray, S.R., 1991. The inorganic geochemical record of the north-west Arabian Sea: a history of productivity variation over the last 400 ky from Sites 722 and 724. Proc. Ocean Drill. Program Sci. Results 117, 409–429.
Shukla, B., Patra, A.K., Panda, R.P., 2013. Primary production in river Birupa, India. Proc. Natl. Acad. Sci., India, Sect. B Biol. Sci. 83 (4), 593–602.
Singh, S.K., France-Lanord, C., 2002. Tracing the distribution of erosion in the Brahmaputra watershed from isotopic compositions of stream sediments. Earth Planet. Sci. Lett. 202 (3), 645–662.
Singh, S.K., Sarin, M.M., France-Lanord, C., 2005. Chemical erosion in the eastern Himalaya: major ion composition of the Brahmaputra and $\delta^{13}C$ of dissolved inorganic carbon. Geochim. Cosmochim. Acta 69 (14), 3573–3588.
Singh, S.K., Rai, S.K., Krishnaswami, S., 2008. Sr and Nd isotopes in river sediments from the Ganga Basin: sediment provenance and spatial variability in physical erosion. J. Geophys. Res. Earth Surf. 113.
Spicer, R.A., Harris, N.B.W., Widdowson, M., Herman, A.B., Guo, S., Valdes, P.J., Wolfe, J.A., Kelley, S.P., 2003. Constant elevation of southern Tibet over the past 15 million years. Nature 421, 622–624.
Subramanian, V., 1987. Environmental geochemistry of Indian river basins-a review. J. Geol. Soc. India 29, 205–220.
Tamburrino, S., Insinga, D.D., Sprovieri, M., Petrosino, P., Tiepolo, M., 2012. Major and trace element characterization of tephra layers offshore Pantelleria Island: insights into the last 200 ka of volcanic activity and contribution to the Mediterranean tephrochronology. J. Quat. Sci. 27, 129–140.
Taylor, S.R., McLennan, S.M., 1985. The Continental Crust: Its Composition and Evolution. Blackwell Scientific Publications, Oxford.
Thomas, D.J., Via, R.K., 2007. Neogene evolution of Atlantic thermohaline circulation: perspective from Walvis Ridge, southeastern Atlantic Ocean. Paleoceanography 22.
Tremblay, M.M., Fox, M., Schmidt, J.L., Tripathy-Lang, A., Wielicki, M.M., Harrison, T.M., Zeitler, P.K., Shuster, D.L., 2015. Erosion in southern Tibet shut down at ~10 Ma due to enhanced rock uplift within the Himalaya. Proc. Natl. Acad. Sci. 112 (39), 12030–12035.
Tribovillard, N., Algeo, T.J., Lyons, T., Riboulleau, A., 2006. Trace metals as paleoredox and paleoproductivity proxies: an update. Chem. Geol. 232 (1), 12–32.
Tripathi, S., Tiwari, M., Lee, J., Khim, B.K., Expedition, I.O.D.P., 2017. First evidence of denitrification Vis-à-Vis monsoon in the Arabian Sea since Late Miocene. Sci. Rep. 7.
Tripathy, G.R., Singh, S.K., Ramaswamy, V., 2014. Major and trace element geochemistry of Bay of Bengal sediments: implications to provenances and their controlling factors. Palaeogeogr. Palaeoclimatol. Palaeoecol. 397, 20–30.
Von Breymann, M.T., Emeis, K.C., Camerlenghi, A., 1990. Geochemistry of sediments from the Peru upwelling area: results from sites 680, 682, 685, and 6881. Proc. Ocean Drill. Program Sci. Results 112, 491–503.
Wan, S., Li, A., Clift, P.D., Stuut, J.B.W., 2007. Development of the East Asian monsoon: mineralogical and sedimentologic records in the northern South China Sea since 20 Ma. Palaeogeogr. Palaeoclimatol. Palaeoecol. 254 (3), 561–582.
Wang, Y.L., Liu, Y.G., Schmitt, R.A., 1986. Rare earth geochemistry of south Atlantic deep sediments, Ce anomaly change at 54 My. Geochim. Cosmochim. Acta 50, 1337–1355.
Wehausen, R., Brumsack, H.J., 1999. Cyclic variations in the chemical composition of eastern Mediterranean Pliocene sediments: a key for understanding sapropel formation. Mar. Geol. 153, 161–176.
Woodruff, F., Douglas, R.G., 1981. Response of deep-sea benthic foraminifera to Miocene paleoclimatic events, DSDP Site 289. Mar. Micropaleontol. 6 (5–6), 617–632.
Woodward, E.M.S., Rees, A.P., Stephens, J.A., 1999. The influence of the south-west monsoon upon the nutrient biogeochemistry of the Arabian Sea. Deep-Sea Res. II Top. Stud. Oceanogr. 46 (3–4), 571–591.
Yang, S., Jiang, S., Ling, H., Xia, X., Sun, M., Wang, D., 2007. Sr-Nd isotopic compositions of the Changjiang sediments: Implications for tracing sediment sources. Sci. China Ser. D Earth Sci. 50 (10), 1556–1565.
Zheng, Y., Anderson, R.F., van Geen, A., Kuwabara, J., 2000. Authigenic molybdenum formation in marine sediments: a link to pore water sulfide in the Santa Barbara Basin. Geochim. Cosmochim. Acta 64 (24), 4165–4178.
Zhisheng, A., Kutzbach, J.E., Prell, W.L., Porter, S.C., 2001. Evolution of Asian monsoons and phased uplift of the Himalaya–Tibetan Plateau since Late Miocene times. Nature 411, 62–66.